We have confirmed that the meta data below are true and correct.

Metadata of the article that will be visualized in OnlineFirst

ArticleTitle	Estimation of baroclinic tide energy available for deep ocean mixing based on three-dimensional global numerical simulations	
Article Sub-Title		
Article CopyRight	The Oceanographic Society of Japan and Springer (This will be the copyright line in the final PDF)	
Journal Name	Journal of Oceanography	
Corresponding Author	Family Name	**Niwa**
	Particle	
	Given Name	**Yoshihiro**
	Suffix	
	Division	Department of Earth and Planetary Science, Graduate School of Science
	Organization	The University of Tokyo
	Address	7-3-1, Hongo, Bunkyo-ku, Tokyo, 113-0033, Japan
	Email	niwa@eps.s.u-tokyo.ac.jp
Author	Family Name	**Hibiya**
	Particle	
	Given Name	**Toshiyuki**
	Suffix	
	Division	Department of Earth and Planetary Science, Graduate School of Science
	Organization	The University of Tokyo
	Address	7-3-1, Hongo, Bunkyo-ku, Tokyo, 113-0033, Japan
	Email	
Schedule	Received	22 March 2011
	Revised	11 June 2011
	Accepted	22 June 2011

Abstract

The global distributions of the major semidiurnal (M_2 and S_2) and diurnal (K_1 and O_1) baroclinic tide energy are investigated using a hydrostatic sigma-coordinate numerical model. A series of numerical simulations using various horizontal grid spacings of 1/15–1/5° show that generation of energetic baroclinic tides is restricted over representative prominent topographic features. For example, nearly half of the diurnal (K_1 and O_1) baroclinic tide energy is excited a[illegible] Pacific from the Aleutian Islands down to the Indonesian Archipelago [illegible]y conversion from the barotropic to baroclinic tides is very sensitive to the horizontal grid spacing as well as the resolution of the model bottom topography; the conversion rate integrated over the global ocean increases exponentially as the model grid spacing is reduced. Extrapolating the calculated results in the limit of zero grid spacing yields the estimate of the global conversion rate to be 1105 GW (821, 145, 102, 53 GW for M_2, S_2, K_1, and O_1 tidal constituents, respectively). The amount of baroclinic tide energy dissipated in the open ocean below a depth of 1000 m, in particular, is estimated to be 500–600 GW, which is comparable to the mixing energy estimated by Webb and Suginohara (Nature 409:37, 2001) as needed to sustain the global overturning circulation.

Change to "shows"

Keywords (separated by '-')	Baroclinic tide - Deep ocean mixing - Global overturning circulation
Footnote Information	

Journal: 10872
Article: 52

Author Query Form

Springer
the language of science

Please ensure you fill out your response to the queries raised below and return this form along with your corrections

Dear Author

During the process of typesetting your article, the following queries have arisen. Please check your typeset proof carefully against the queries listed below and mark the necessary changes either directly on the proof/online grid or in the 'Author's response' area provided below

Query	Details required	Author's response
1.	Please check the term "subinertial" and amend as necessary.	The term "subinertial" is OK.
2.	Please check the totals "479" and "665" in Table 1 (totals are 478 and 664, respectively).	The totals "479" and "665" are correct, because Table 1 shows the nearest integer numbers obtained by rounding off decimal part.

J Oceanogr
DOI 10.1007/s10872-011-0052-

The quality of figures (Figs. 1-8) in the proof manuscript is not sufficiently high, so please replace all the figures with the higher-resolution ones which are downloadable from http://www-aos.eps.s.u-tokyo.ac.jp/~niwa/JO/figures/

ORIGINAL ARTICLE

Estimation of baroclinic tide energy available for deep ocean mixing based on three-dimensional global numerical simulations

Yoshihiro Niwa · Toshiyuki Hibiya

Received: 22 March 2011 / Revised: 11 June 2011 / Accepted: 22 June 2011

Abstract The global distributions of the major semidiurnal (M_2 and S_2) and diurnal (K_1 and O_1) baroclinic tide energy are investigated using a hydrostatic sigma-coordinate numerical model. A series of numerical simulations using various horizontal grid spacings of 1/15–1/5° show that generation of energetic baroclinic tides is restricted over representative prominent topographic features. For example, nearly half of the diurnal (K_1 and O_1) baroclinic tide energy is excited along the western boundary of the North Pacific from the Aleutian Islands down to the Indonesian Archipelago. It is also found that the rate of energy conversion from the barotropic to baroclinic tides is very sensitive to the horizontal grid spacing as well as the resolution of the model bottom topography; the conversion rate integrated over the global ocean increases exponentially as the model grid spacing is reduced. Extrapolating the calculated results in the limit of zero grid spacing yields the estimate of the global conversion rate to be 1105 GW (821, 145, 102, 53 GW for M_2, S_2, K_1, and O_1 tidal constituents, respectively). The amount of baroclinic tide energy dissipated in the open ocean below a depth of 1000 m, in particular, is estimated to be 500–600 GW, which is comparable to the mixing energy estimated by Webb and Suginohara (Nature 409:37, 2001) as needed to sustain the global overturning circulation.

Keywords Baroclinic tide · Deep ocean mixing · Global overturning circulation

Change to "shows"

1 Introduction

Baroclinic tides are ubiquitous phenomena in the stratified ocean. They are generated by barotropic tidal currents flowing over a rough ocean bottom such as mid-ocean ridges and continental shelf slopes; the stratified water is [illegible]ically displaced up and down and part of the [illegible]c tide energy is converted into baroclinic tide energy. Baroclinic tides have a large vertical displacement of density surfaces in the ocean interior with amplitudes reaching several tens of meters and are characterized by relatively short horizontal wavelengths of the order of 100 km.

Baroclinic tides have a strong influence on the global overturning circulation and hence on the world's climate, because they are thought to contribute to turbulent mixing in the deep ocean; near the generation sites, the vertical shear of horizontal currents associated with baroclinic tides can be strong enough to cause shear instability leading to locally enhanced turbulent mixing. Turbulent mixing can also even be induced far from the generation sites, because propagating baroclinic tides nonlinearly interact with the [illegible] scales inducing shear instability. The induced turbulent mixing transfers heat from the surface down to the dense deep water that originates from high latitudes, causing it to upwell back to the sea surface at low and mid latitudes. Actually, ocean general circulation models (OGCMs) (e.g., Hasumi and Suginohara 1999) demonstrate that the rate and spatial distribution of turbulent mixing can strongly control the fundamental features of the global overturning circulation such as flow and density structures as well as the transport of heat and chemical tracers. Thus, understanding the global distribution of baroclinic tide energy is

Please set as "…can also be induced even far from …."

Y. Niwa (✉) · T. Hibiya
Department of Earth and Planetary Science,
Graduate School of Science, The University of Tokyo,
7-3-1, Hongo, Bunkyo-ku, Tokyo 113-0033, Japan
e-mail: niwa@eps.s.u-tokyo.ac.jp

Journal : Large 10872 | Dispatch : 8-7-2011 | Pages : 10
Article No. : 52 | LE | TYPESET
MS Code : JO52_1293 | CP | DISK

essential for accurate modeling of the ocean general circulation.

Accurate estimates of baroclinic tide energy are also crucial for understanding the energy balance of the global overturning circulation. Munk and Wunsch (1998) estimated that 2100 GW (1 GW = 10^9 W) of mixing energy is required to pull up 30 Sv of the dense deep water below a depth of 1000 m (the typical depth of the main thermocline) and postulated that nearly half of that energy was supplied by baroclinic tides and the remaining half by the wind-induced internal waves. On the other hand, Webb and Suginohara (2001) suggested that the Ekman suction in the Southern Ocean might pull up about half of the deep water formed in the North Atlantic to the sea surface, reducing the required mixing energy to as low as 600 GW. It still remains a matter of debate as to which of these mixing energy analyses is more convincing (Kuhlbrodt et al. 2007). An important step toward answering this question is to accurately estimate the amount of baroclinic tide energy available for deep ocean mixing.

Many studies have been carried out to predict the global distribution of the rate of energy conversion from the barotoropic to baroclinic tides (Sjöberg and Stigebrandt 1992; Morozov 1995; Kantha and Tierney 1997; Jayne and St. Laurent 2001; Nycander 2005). However, estimates of the global baroclinic conversion rate derived from these studies vary widely (more than ±50%), because they are based on simplified analytical models under idealized assumptions whose applicability to the real ocean is questionable. Using the TOPEX/Poseidon altimetry data and an inverse tidal model, on the other hand, Egbert and Ray (2000) estimated that roughly 1000 GW or 20–30% of the global barotropic tide energy is dissipated within the open ocean including the region of rough seafloor topography. But their inverse tidal model cannot discriminate between the dissipation due to baroclinic tide generation and the direct frictional dissipation within the bottom boundary layer (BBL). Thus, to accurately estimate the baroclinic tide energy available for deep ocean mixing, numerical studies based on primitive Navier–Stokes equations are most desirable. To date, only one numerical study attempting to simulate the global baroclinic tide field has been carried out—that by Simmons et al. (2004), but they were concerned only with the most dominant M_2 tidal response for a horizontally uniform idealized density stratification. Furthermore, vertical grid resolutions in their numerical model (2 or 10 layers) are too coarse to adequately resolve high vertical-mode baroclinic tides.

In the present study, we investigate the spatial distribution of the major semidiurnal (M_2 and S_2) and diurnal (K_1 and O_1) baroclinic tide energy using a fine-grid three-dimensional numerical model incorporating realistic bottom topography, density stratification, and barotropic tidal forcing. In order to accurately estimate the rate of energy conversion into baroclinic tides, in particular, a series of numerical simulations with various horizontal grid spacings of 1/5–1/15° are conducted to examine the sensitivity of the calculated results to the model grid spacing as well as the resolution of the model bottom topography.

Change to "is"

2 Numerical experiment

Figure 1 shows the model domain that covers the global ocean from 80°S to 80°N, excluding the central part of the Arctic Ocean and the shallow shelf regions near the Antarctic continent.

The governing equations are the full three-dimensional Navier–Stokes equations under hydrostatic and Boussinesq approximations. The vertical eddy viscosity and diffusivity are parameterized following the Richardson number formulation of Pacanowski and Philander (1981). Furthermore, taking into account the decay of propagating baroclinic tides due to their nonlinear interactions with the background Garrett–Munk internal waves (Munk 1981) as well as mesoscale eddies, we include artificial linear damping terms for the depth-varying horizontal velocities and the deviations of potential temperature and salinity from the basic fields. In the present study, the damping time is set to be 30 days which is estimated based on the analysis of tidal current data obtained from long-term mooring observations (the details of the data analysis will be reported elsewhere).

The governing equations are numerically integrated using the Princeton Ocean Model (Blumberg and Mellor 1987). To examine the sensitivity of the model results to the horizontal grid spacing as well as the resolution of the model bottom topography, a set of numerical experiments are carried out using five different horizontal grid spacings, namely, 1/5°, 1/6°, 2/15°, 1/10°, and 1/15°. In all cases, 41 sigma levels are assumed in the vertical with a logarithmic near the sea surface. For details of the governing equations and the numerical model, readers are referred to Niwa and Hibiya (2004).

Change to "is"

For each numerical experiment, the model topography is constructed by averaging the 2-min (1/30°) gridded global bathymetric data of ETOPO2 (Smith and Sandwell 1997) within each model grid cell so as to increase the resolution of the model topography with the decrease of the model grid spacing. The basic temperature and salinity fields are obtained from the annual mean data of the National Oceanographic Data Center's *World Ocean Atlas* (Levitus and Boyer 1994; Levitus et al. 1994).

The model is forced by the tidal potential forcing of four major semidiurnal and diurnal astronomical tidal

Journal : Large 10872 | Dispatch : 8-7-2011 | Pages : 10
Article No. : 52 | LE | TYPESET
MS Code : JO52_1293 | CP | DISK

Short title should be
"Baroclinic tide energy for deep ocean mixing"

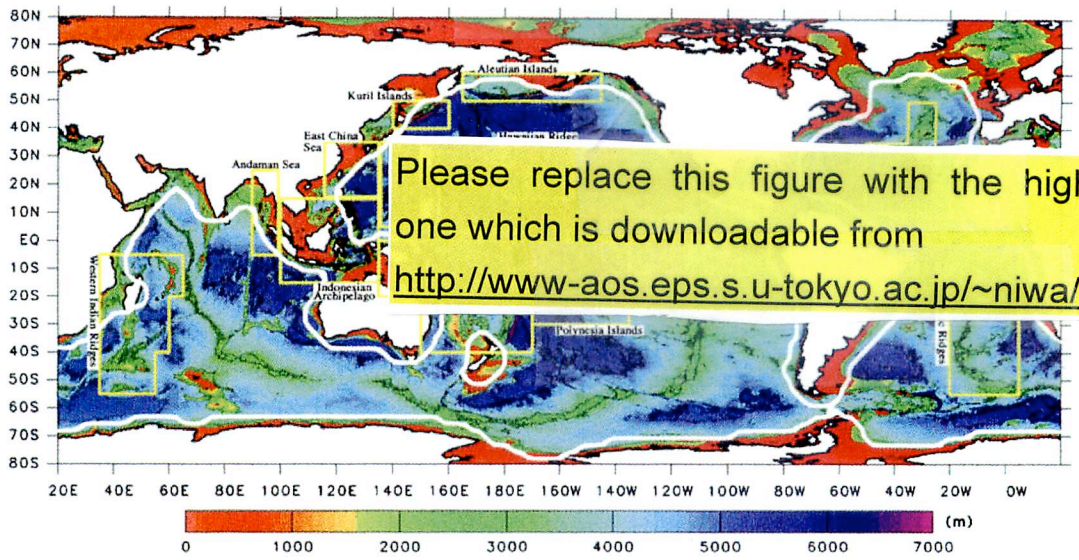

Please replace this figure with the higher-resolution one which is downloadable from
http://www-aos.eps.s.u-tokyo.ac.jp/~niwa/JO/figures/

Fig. 1 The whole model domain and the bathymetry. The regions including the prominent topographic features referred to in the text are indicated by *yellow lined squares*. The *thick white line* indicates the boundary between the open ocean and the coastal and marginal seas

constituents (M_2, S_2, K_1 and O_1). Furthermore, in order to reproduce the realistic barotropic tidal field, we assimilate the barotropic surface tidal elevation data of Matsumoto et al. (2000). The model is driven by the M_2, S_2, K_1 and O_1 tidal forcing for 60 days from an initial state of rest with time steps of 30 and 3.75 s for the baroclinic and barotropic modes, respectively. The calculated time series data for the last 20 days are harmonically analyzed to obtain the amplitude and phase of each tidal constituent. In order to extract the information about baroclinic tides, we subtract the depth-averaged tidal currents from the calculated tidal currents.

3 Results

3.1 Global distribution of baroclinic tide energy

Figure 2a shows the global distribution of the depth-integrated kinetic energy of the semidiurnal (M_2 and S_2) baroclinic tides obtained using the finest horizontal grid spacing of 1/15°. It should be noted that, u… stated, the calculated results using the finest (1/15°) will be shown hereafter, because the qualitative features are the same for all the other results using the coarser horizontal grids. Figure 2a indicates that the spatial distribution of the semidiurnal baroclinic tide energy is highly inhomogeneous reflecting that of the prominent topographic features. Particularly high energy levels are found in the western Pacific Ocean, the western Indian Ocean, and the Mid-Atlantic Ocean, which are 2–3 orders of magnitude higher than those in the Southern Ocean and the eastern Pacific Ocean.

To examine the generation of baroclinic tides more quantitatively, we calculate the depth-integrated energy conversion rate from the barotropic to baroclinic tides (Niwa and Hibiya 2004) defined as

$$C(x,y) \equiv \int_{-H}^{0} g\overline{\rho' w_s}\,\mathrm{d}z \qquad (1)$$

where H is the total depth of the water column, g is the acceleration due to gravity, ρ' is the density deviation from the basic field associated with baroclinic tide motions, w_s is the vertical velocity resulting from the interaction of depth-averaged tidal currents with bottom topographic features, and the overbar denotes the temporal average over one tidal period. In Fig. 3, the depth-integrated energy conversion rate from the barotropic to baroclinic tides is further integrated within each 5°-latitude by 5°-longitude grid area to identify the important generation regions.

We can see in Fig. 3a that the semidiurnal baroclinic …erated in the coastal and marginal …minent topographic features in the Indonesian Archipelago and over the continental shelf slope in the East China Sea and the Andaman Sea. Energetic baroclinic tides can also be generated in the open ocean along the steep topographic features such as the Hawaiian Ridge, the Izu-Ogasawara Ridge, the Western-Indian Ridges, and the Mid-Atlantic Ridges, and over the seamounts in the Micronesia Islands and the Polynesia Islands.

Please change to "slopes"

Journal : Large 10872 | Dispatch : 8-7-2011 | Pages : 10
Article No. : 52 | LE | TYPESET
MS Code : JO52_1293 | CP | DISK

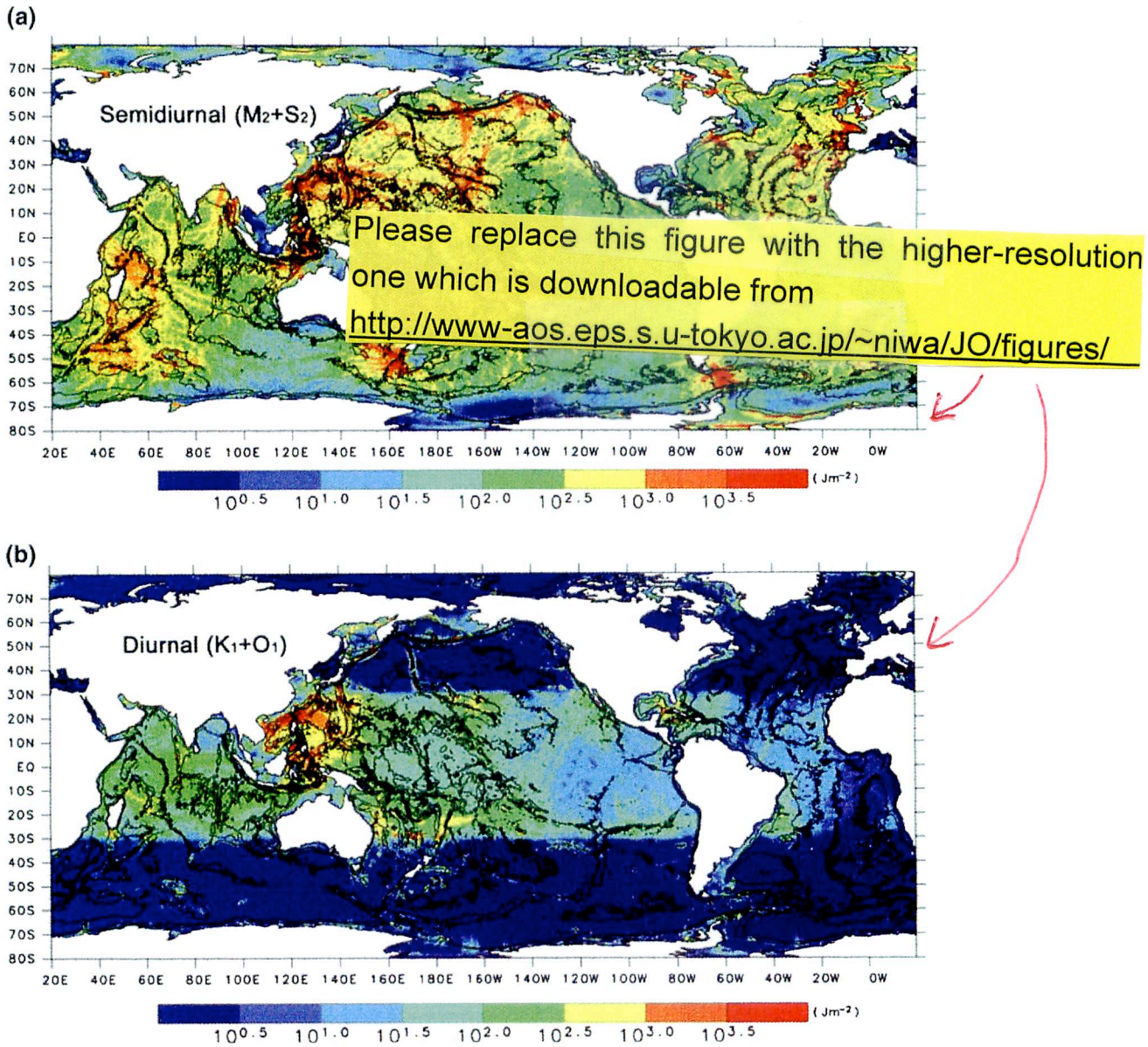

Fig. 2 **a** The depth-integrated kinetic energy of the semidiurnal (M_2 and S_2) baroclinic tide. **b** As in **a** but for the diurnal (K_1 and O_1) baroclinic tide. The results of the numerical simulation for a horizontal grid spacing of 1/15° are shown

Figure 2b shows the spatial distribution of the diurnal (K_1 and O_1) baroclinic tide energy. We can see that the diurnal baroclinic tide energy is mostly limited to equatorward of about 30°N/S, because each linear diurnal baroclinic tide cannot propagate freely poleward of the critical latitude where the diurnal tidal frequency becomes subinertial (the exact critical latitudes for K_1 and O_1 baroclinic tides are 30.00°N/S and 27.37°N/S, respectively). Energetic diurnal baroclinic tides are also excited at high latitudes beyond the critical latitudes such as in the Aleutian Islands and the Kuril Islands in the form of coastal-trapped internal waves propagating along the steep topographic features (Tanaka et al. 2010) and/or short internal waves generated over topographic features in the highly constricted tidal straits (Nakamura et al. 2010). Figure 3b shows that the generation of large diurnal baroclinic tides is mostly limited to along the western boundary of the North Pacific from the Aleutian Islands down to the Indonesian Archipelago where nearly half of the global diurnal baroclinic tide energy is found to be excited.

Journal : Large 10872 | Dispatch : 8-7-2011 | Pages : 10
Article No. : 52 | LE | TYPESET
MS Code : JO52_1293 | CP | DISK

Short title should be
"Baroclinic tide energy for deep ocean mixing"

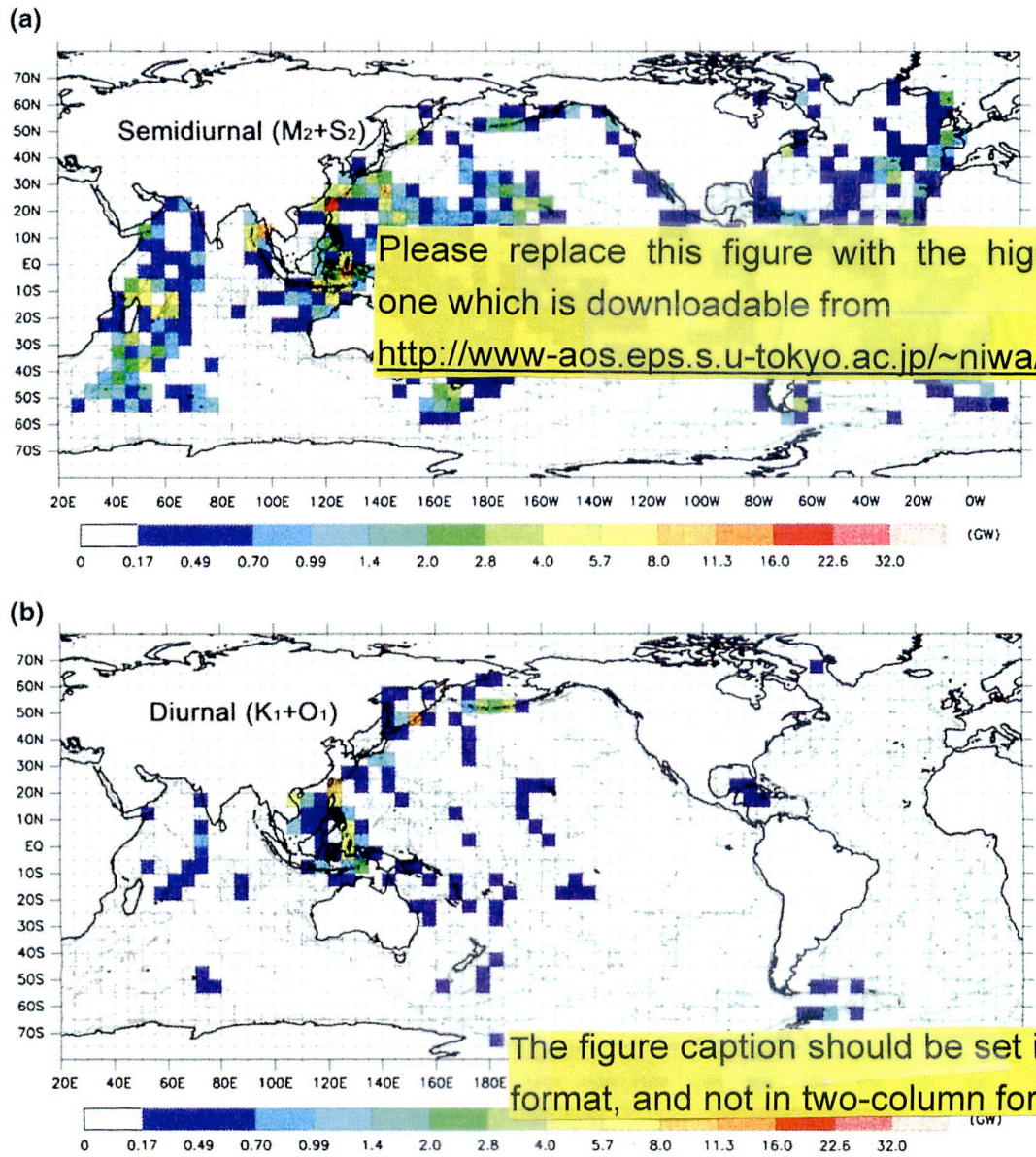

Please replace this figure with the higher-resolution one which is downloadable from
http://www-aos.eps.s.u-tokyo.ac.jp/~niwa/JO/figures/

The figure caption should be set in one-column format, and not in two-column format.

Fig. 3 **a** The depth-integrated energy conversion rate from the barotropic to baroclinic tides for the semidiurnal (M_2 and S_2) tidal constituents. **b** As in **a** but for the diurnal (K_1 and O_1) tidal constituents. The results of the numerical simulation for a horizontal grid spacing of 1/15° are shown

3.2 Estimation of global energy conversion rate from the barotropic to baroclinic tides

The rate of energy conversion from the barotropic to baroclinic tides integrated over the global ocean is estimated to be 782 GW (553, 96, 87, and 46 GW for the individual tidal constituents, respectively) for the high-resolution (1/15°). This value does not change appreciably even if the linear damping time scale is changed or the annual mean temperature and salinity fields are replaced by the corresponding summer/winter climatological fields. The global baroclinic conversion rate is, however, very sensitive to the horizontal grid spacing and hence the resolution of the model bottom topography (Table 1); decreasing the horizontal grid spacing from 1/5° to 1/15° increases the baroclinic conversion rate linearly as the horizontal grid spacing is reduced; This exponential relationship primarily reflects the similar relationship found between the

Please change to the colon separator (:),
"…(Table 1); decreasing…" →"…(Table 1): decreasing…"

Uncapitalize this word; "This"→"this"

Journal : Large 10872 | Dispatch : 8-7-2011 | Pages : 10
Article No. : 52 | LE | TYPESET
MS Code : JO52_1293 | CP | DISK

Please set this caption below or above Table 1.

Table 1 should be centered.

Table 1 The globally integrated energy conversion rate from the barotropic to baroclinic tides obtained from each of the numerical simulations with various horizontal grid spacings, together with that obtained from the extrapolation in the limit of zero grid spacing

Horizontal grid spacing (Δx, °)	Global baroclinic conversion rate (GW)				
	M_2	S_2	K_1	O_1	Sum of M_2, S_2, K_1 and O_1
1/5	255	43	63	34	394
1/6	322	53	67	36	479
1/7.5	387	[illegible]	[illegible]	[illegible]	564
1/10	[illegible]	[illegible]	[illegible]	[illegible]	665
1/15	[illegible]	96	87	46	782
0	Extrapolated global baroclinic conversion rate at $\Delta x = 0$ (GW)				
	821 ± 53	145 ± 4	102 ± 2	53 ± 1	1105 ± 39

Please move down "0" by one row

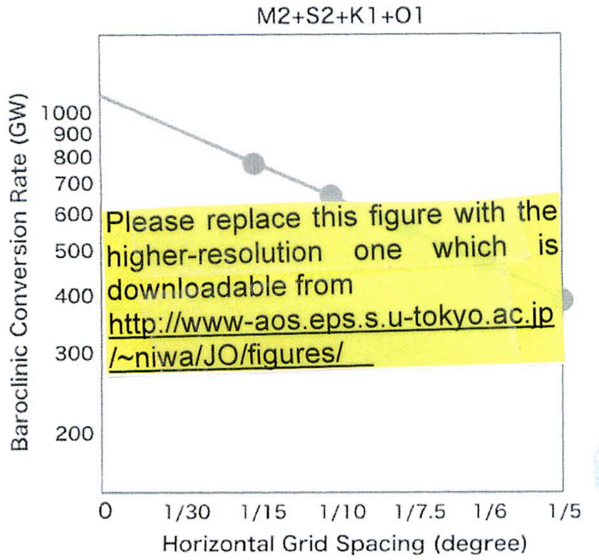

Please replace this figure with the higher-resolution one which is downloadable from http://www-aos.eps.s.u-tokyo.ac.jp/~niwa/JO/figures/

Fig. 4 Plots of the globally integrated energy conversion rate from the barotropic to baroclinic tides for the major four tidal constituents (M_2, S_2, K_1 and O_1) on a logarithm scale against the horizontal grid spacing for each of the numerical simulations. The least-squares fit is shown

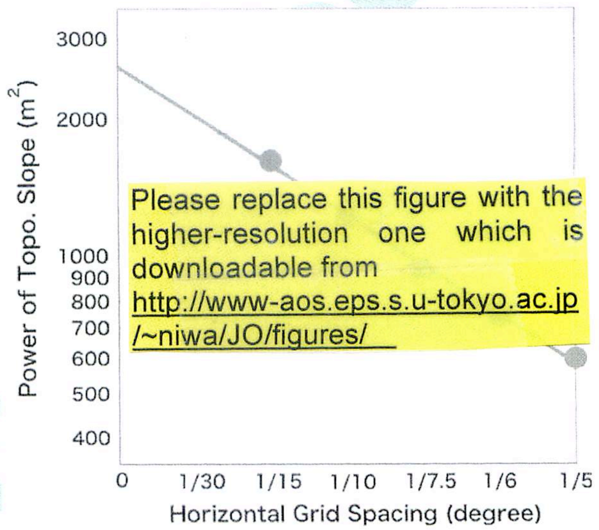

Please replace this figure with the higher-resolution one which is downloadable from http://www-aos.eps.s.u-tokyo.ac.jp/~niwa/JO/figures/

Fig. 5 Plots of the globally integrated power of the bottom topography slope on a logarithm scale against the horizontal grid spacing for each of the numerical simulations. The least-squares fit is shown

horizontal grid spacing in each experiment and [illegible] sponding globally integrated power of the slope o[illegible] tom topographic features ($\int |\nabla H|^2 dxdy$) (Fig. 5), the amplitudes of w_s and ρ' in Eq. (1) both have a positive linear correlation with the bottom slope $|\nabla H|$ over the prominent topographic features.

Please set as $\iint_{\mathrm{global}} |\nabla H| \, dx\, dy$

It sho[illegible] clinic c[illegible] grid spa[illegible] topograp[illegible] internal tides. In spite of this uncertainty, we extrapolate the least-squares fitting in Fig. 4 to the limit of zero grid spacing to estimate the global baroclinic conversion rate to be 1105 GW (821, 145, 102, 53 GW for M_2, S_2, K_1, and O_1 tidal constituents, respectively) (Table 1) which corresponds to 32% of the global tidal energy dissipation rate of 3500 GW. We should bear in mind, however, that, so long as there is the uncertainty mentioned above, this value [illegible] available for deep ocean mixing.

Please remove the word 'estimated' and set as "…the aforementioned global baroclinic tide energy…"

It should be noted that the aforementioned estimated global baroclinic tide energy is not fully available to sustain the global overturning circulation, because turbulent mixing that occurs in the coastal and marginal seas and/or in the upper ocean above the main thermocline does not come into play in pulling up the dense deep water that originates from high latitudes. Therefore, to evaluate the amount of baroclinic tide energy available for deep ocean mixing needed to sustain the global overturning circulation, we have to estimate how much of the baroclinic tide energy propagates outward into the open ocean and dissipates below the main thermocline. For this purpose, we first estimate the depth-integrated dissipation rate of baroclinic

Journal : Large 10872 | Dispatch : 8-7-2011 | Pages : 10
Article No. : 52 | LE | TYPESET
MS Code : JO52_1293 | CP | DISK

Short title should be
"Baroclinic tide energy for deep ocean mixing"

tide energy; assuming the nonlinear advection effect is negligible, it is given by the difference between the energy conversion rate and the energy flux divergence (Niwa and Hibiya 2004), namely,

$$D(x,y) \equiv \int_{-H}^{0} g\overline{\rho' w_s}\,\mathrm{d}z - \int_{-H}^{0} \left[\frac{\partial}{\partial x}\left(\overline{p'u'}\right) + \frac{\partial}{\partial y}\left(\overline{p'v'}\right)\right] \mathrm{d}z \qquad (2)$$

where u' and v' are the eastward and northward velocities and the pressure perturbations associated with baroclinic tide motions, respectively. Note that the energy boundaries

Please set as "where u', v' and p' are"

the global integral of the energy dissipation rate $\iint_{\mathrm{global}} D(x,y)\mathrm{d}x\mathrm{d}y$ is almost the same as that of the conversion rate $\iint_{\mathrm{global}} C(x,y)\mathrm{d}x\mathrm{d}y$. Figures 6a and b show the spatial distribution of the dissipation rate of the semidiurnal (M_2 and S_2) baroclinic tide energy and that of the

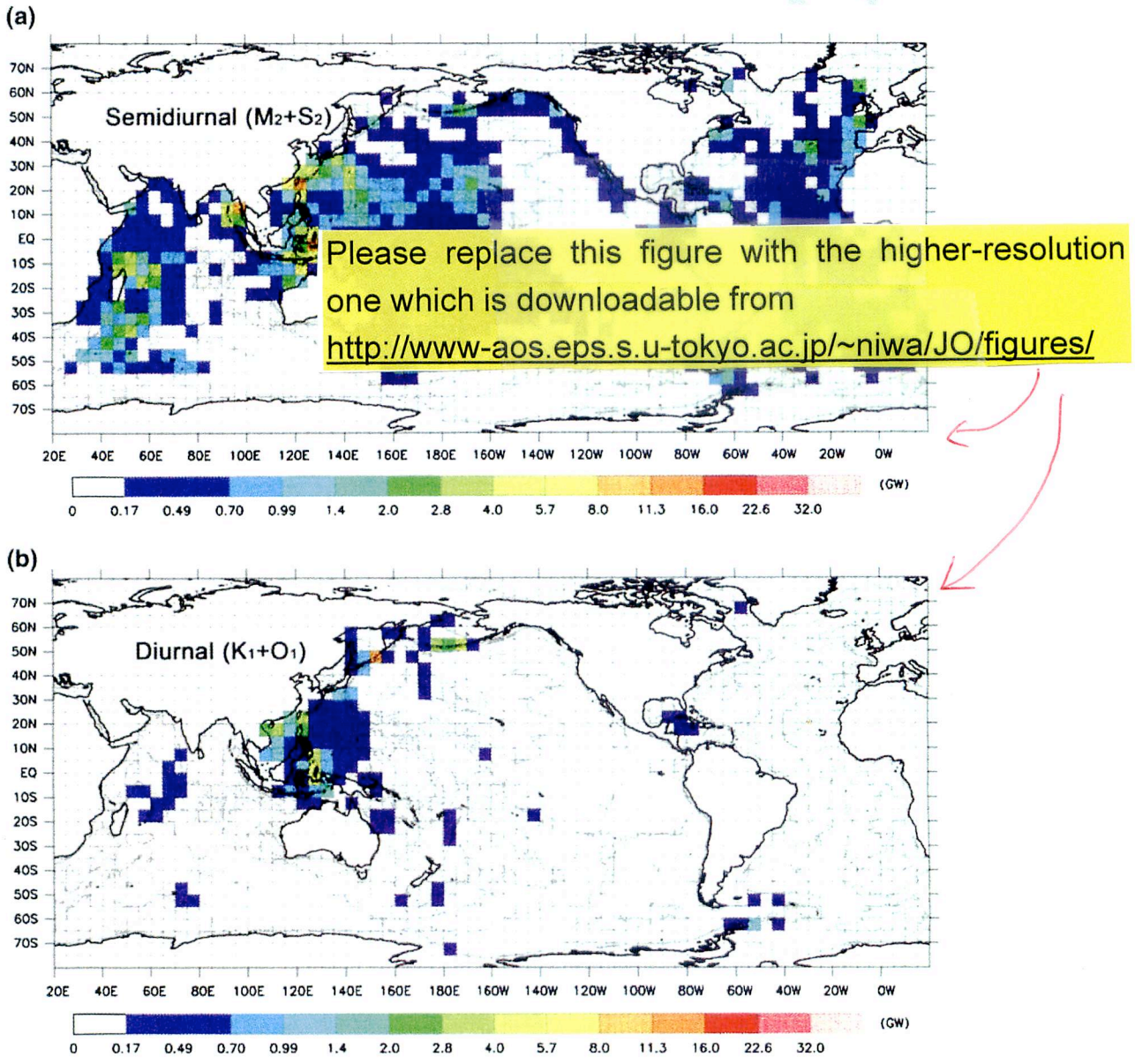

Please replace this figure with the higher-resolution one which is downloadable from
http://www-aos.eps.s.u-tokyo.ac.jp/~niwa/JO/figures/

Fig. 6 **a** The depth-integrated dissipation rate of the baroclinic tide energy for the semidiurnal (M_2 and S_2) tidal constituents. **b** As in **a** but for the diurnal (K_1 and O_1) tidal constituents. The results of the numerical simulation for a horizontal grid spacing of 1/15° are shown

Journal : Large 10872 | Dispatch : 8-7-2011 | Pages : 10
Article No. : 52 | LE | TYPESET
MS Code : JO52_1293 | CP | DISK

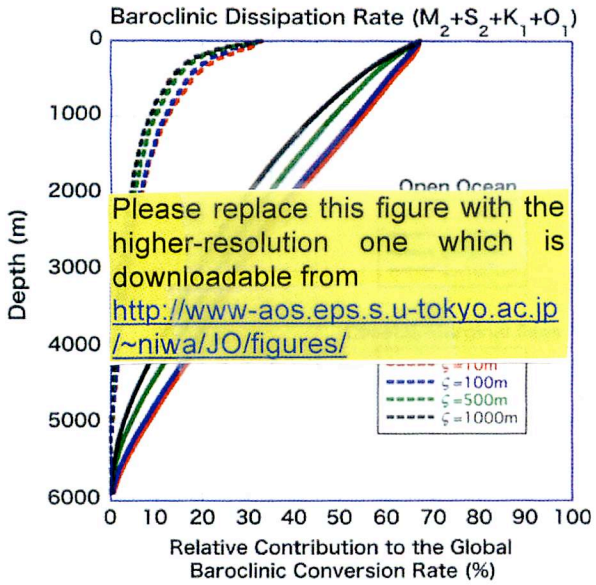

Please replace this figure with the higher-resolution one which is downloadable from http://www-aos.eps.s.u-tokyo.ac.jp/~niwa/JO/figures/

Fig. 7 The cumulative depth distribution of the dissipation rate of baroclinic tide energy for the four major tidal constituents (M_2, S_2, K_1, and O_1) within the open ocean (*solid lines*) and within the coastal and marginal seas (*dotted lines*) which are calculated assuming an exponential vertical structure function with various scale height parameters ς = 10, 100, 500, and 1000 m. Note that each dissipation rate is normalized by the globally integrated baroclinic conversion rate. The boundary between the open ocean and the coastal and marginal seas is shown by the *thick white line* in Fig. 1

Please insert "(Figs 6a and 6b)" here

diurnal (K_1 and O_1) baroclinic tide energy, respectively. We can see that the spatial distribution of the energy dissipation rate is similar to that of the energy conversion rate for each tidal constituent, but extends more outward from each prominent topographic feature as a result of baroclinic tide propagation. If the open ocean and the coastal and marginal seas is defined as shown by the thick white line in Fig. 1, we can extrapolate the total baroclinic dissipation rate within the open ocean (or the coastal and marginal seas) in the limit of zero grid spacing to be 761 (or 345) GW, which is slightly larger (or smaller) than the total baroclinic conversion rate 744 (or 362) GW within the open ocean (or the coastal and marginal seas), which implies that baroclinic tides, on the whole, are carrying their energy from the coastal and marginal seas to the open ocean.

Please insert "(Figs 3a and 3b)" here

Next, we investigate how much of the baroclinic tide energy is dissipated in the open ocean below the depth of the main thermocline (about 1000 m). Recent microstructure measurements (St. Laurent et al. 2002) show the existence of bottom-intensified turbulent mixing associated with breaking of baroclinic tides, the intensity of which decays upwards within a distance of about 500 m from the ocean bottom. Taking this into account, we assume that the depth-integrated dissipation rate D is vertically distributed following a vertical structure function given by

$$\phi(z;H) = \frac{e^{-(H+z)/\varsigma}}{\varsigma(1-e^{-H/\varsigma})} \tag{3}$$

which satisfies $\int_{-H}^{0} \phi(z;H)\mathrm{d}z = 1$. In terms of $\phi(z;H)$, the fraction of baroclinic tide energy that is dissipated in the open ocean at depths greater than $|z|$ can be calculated as

$$F_{\mathrm{open}}(z) = \frac{\iint_{\mathrm{open}} \left[\int_{-H(x,y)}^{z} D(x,y)\phi(z';H(x,y))\mathrm{d}z'\right]\mathrm{d}x\mathrm{d}y}{\iint_{\mathrm{global}} C(x,y)\mathrm{d}x\mathrm{d}y} \tag{4}$$

Recent theoretical and observational studies (Iwamae et al. 2009; Decloedt and Luther 2010) show that ς in the open ocean can vary from several tens to hundreds of meters depending on the characteristic wavelength of small-scale baroclinic tides generated over ocean bottom roughness. Figure 7 shows the plots of $F_{\mathrm{open}}(z)$ (thick solid lines) for the scale height parameters ς = 10, 100, 500, 1000 m, respectively. The same function but for the coastal and marginal seas $F_{\mathrm{coastal}}(z)$ is also plotted in Fig. 7 (thin dotted line). Although the value of $F_{\mathrm{open}}(z)$ at each z decreases as the scale height parameter ς increases, $F_{\mathrm{open}}(z)$ does not change appreciably even if ς is varied over two orders of magnitude. Figure 7 indicates that 45–55% of the global baroclinic tide energy is dissipated in the open ocean below a depth of 1000 m ($F_{\mathrm{open}}(-1000\ \mathrm{m})$). Multiplying this fraction by the global energy conversion rate in the limit of zero grid spacing (1105 GW), we can conclude that 500–600 GW of the energy supplied to the deep ocean mixing which is available to sustain the global overturning circulation.

4 Summary and discussions

In the present study, using a three-dimensional numerical model, we have investigated the global distribution and budget of the semidiurnal and diurnal (M_2, S_2, K_1, and O_1) baroclinic tide energy. It has been shown that the semidiurnal baroclinic tide energy becomes particularly high in the western Pacific Ocean, the western Indian Ocean, and the Mid-Atlantic Ocean reflecting the spatial distribution of the prominent topographic features, whereas the diurnal baroclinic tide energy is mostly limited to along the western coast of the north Pacific Ocean from the Aleutian Islands down to the Indonesian Archipelago.

The sensitivity experiments have shown that the rate of

Please change to "the North Pacific Ocean"

Journal : Large 10872 | Dispatch : 8-7-2011 | Pages : 10
Article No. : 52 | LE | TYPESET
MS Code : JO52_1293 | CP | DISK

strongly depends on the horizontal grid spacing as well as the resolution of the model bottom topography; the energy conversion rate increases exponentially as the horizontal grid spacing is decreased. This clearly indicates the necessity of numerical simulations with much higher grid resolutions incorporating fine-scale bathymetric data such as those obtained by multibeam echo sounder observations. Although very high resolution numerical simulations (horizontal grid spacings less than 1 km) incorporating the multibeam bathymetric data have been carried out for some localized regions (Carter et al. 2008; Zilberman et al. 2009), such high resolution numerical simulations cannot be extended over the global ocean for the moment because of insufficient computer capacity as well as the limitation of multibeam bathymetric data.

In the present study, we have instead estimated the baroclinic energy conversion rate in the limit of zero grid s[illegible]ential relationship found b[illegible]onversion rate and the horizontal grid spacing. Figure 8 depicts the global tidal energy budget obtained from the present study. We have found that the 3500 GW of global barotropic tidal energy is [illegible] over the [illegible] about

Please remove "the"

Please set this caption below Figure 8.

Fig. 8 The global tidal energy budget estimated in the present study

750 GW of which is dissipated within the open ocean (defined as the region outside the coastal and marginal seas).

We have also found that 45–55% of the global baroclinic tide energy is dissipated below a depth of 1000 m (the typical depth of the main thermocline) in the open ocean so that 500–600 GW of the baroclinic tide energy is estimated to be available for deep ocean mixing. This value is just barely 30% of 2100 GW, namely, the energy required to sustain the global overturning circulation estimated by Munk and Wunsch (1998), but it is consistent with the estimate by Webb and Suginohara (2001) who insisted that the required mixing energy can be reduced down to 600 GW by considering the existence of the Ekman suction in the Southern Ocean adiabatically pulling up about half of the North Atlantic Deep Water (NADW).

Munk and Wunsch (1998) have argued that the remaining energy for deep ocean mixing could be supplied by the wind-induced internal waves. However, recent numerical simulations by Furuichi et al. (2008) and Zhai et al. (2009) both demonstrated that the total wind-induced near-inertial wave energy available for deep ocean mixing was limited to, at most, 100 GW, because more than 70% [illegible] energy was

Figure 8 should be centered.

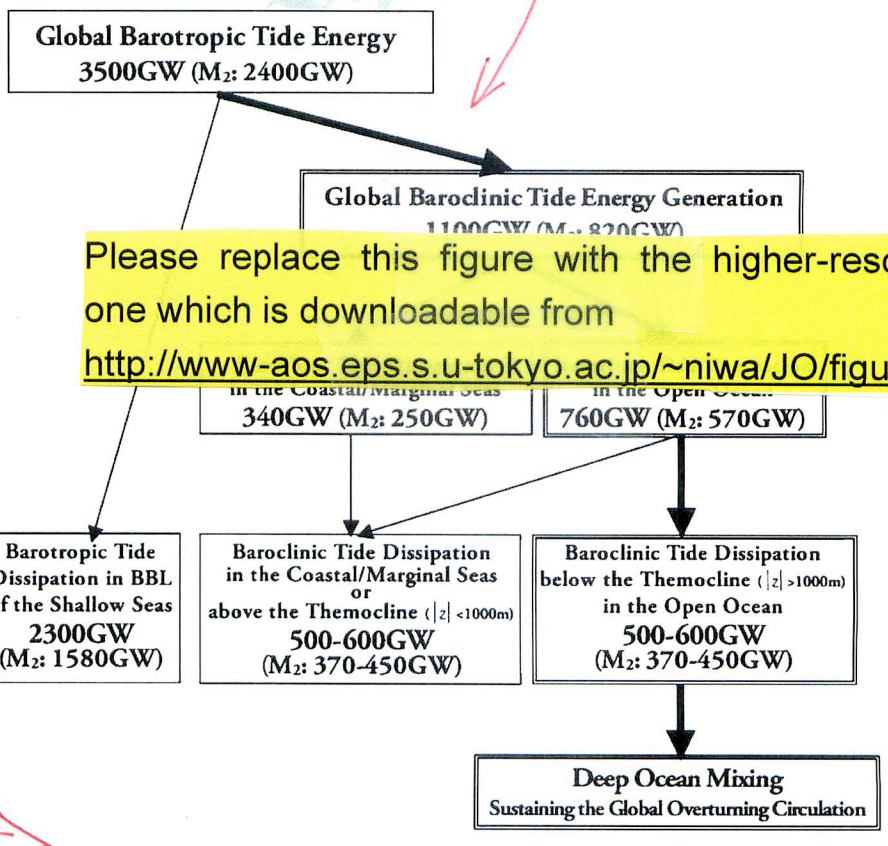

Please replace this figure with the higher-resolution one which is downloadable from
http://www-aos.eps.s.u-tokyo.ac.jp/~niwa/JO/figures/

Journal : Large 10872 | Dispatch : 8-7-2011 | Pages : 10
Article No. : 52 | ☐ LE | ☐ TYPESET
MS Code : JO52_1293 | ☑ CP | ☑ DISK

dissipated within the top 200 m and hence not available for turbulent mixing at greater depths. Even adding the contribution from the wind-induced internal waves, therefore, they estimated the total energy available for deep ocean mixing to be 600–700 GW. This seems to support the validity of the argument of Webb and Suginohara (2001) rather than that of Munk and Wunsch (1998).

Alternatively, this might suggest the existence of "missing energy sources" for deep ocean mixing such as internal waves generated by geostrophic flows interacting with topographic features, internal waves generated through geostrophic adjustment processes, and stirring of the water column by swimming animals in the ocean (Ferrari and Wunsch 2009). Another possibility is that the upwelling transport rate of dense deep water ~ 30 Sv assumed by Munk and Wunsch (1998) might be overestimated. Actually, Schmitz (1995) suggested a much lower value of 14–17 Sv. To close the energy budget for the global overturning circulation, therefore, an accurate estimate of the upwelling transport rate of dense deep water is necessary besides the search for possible energy sources of "missing mixing".

Finally, it should be pointed out that the budget of the global baroclinic tide energy presented in this study is completely based on the empirical relationship found between the baroclinic conversion rate and the horizontal grid spacing. To ensure the validity of the present study, the physical background behind this empirical relationship as well as the limitations of its applicability to the real ocean should be clarified, which also remains to be studied in the future.

References

Blumberg AF, Mellor GL (1987) A description of a three-dimensional coastal ocean circulation model. In: Heaps N (ed) Three-dimensional coastal ocean models. AGU, Washington, DC

Carter GS, Merrifield MA, Becker JM, Katsumata K, Gregg MC, Luther DS, Levine MD, Boyd TJ, Firing YL (2008) Energetics of M_2 barotropic-to-baroclinic tidal conversion at the Hawaiian Islands. J Phys Oceanogr 38(10):2205–2223

Decloedt T, Luther DS (2010) On a simple empirical parameterization of topography-catalyzed diapycnal mixing in the abyssal ocean. J Phys Oceanogr 40(3):487–508

Egbert GD, Ray RD (2000) Significant dissipation of tidal energy in the deep ocean inferred from satellite altimeter data. Nature 405(6788):775–778

Ferrari R, Wunsch C (2009) Ocean circulation kinetic energy: reservoirs, sources and sinks. Annu Rev Fluid Mech 41:253–282

Furuichi N, Hibiya T, Niwa N (2008) Model-predicted distribution of wind-induced internal wave energy in the world's oceans. J Geophys Res 113(C09034). doi:10.1029/2008JC004768

Hasumi H, Suginohara N (1999) Effects of locally enhanced vertical diffusivity over rough bathymetry on the world ocean circulation. J Geophys Res 104(C10):23367–23374

Iwamae N, Hibiya T, Watanabe M (2009) Numerical study of the bottom-intensified tidal mixing using an "eikonal approach". J Geophys Res 114(C05022). doi:10.1029/2008JC005130

Jayne SR, St. Laurent LC (2001) Parameterizing tidal dissipation over rough topography. Geophys Res Lett 28(5):811–814

Kantha LH, Tierney CC (1997) Global baroclinic tides. Prog Oceanogr 40:163–178

Kuhlbrodt T, Griesel A, Montoya M, Levermann A, Hofmann M, Rahmstorf S (2007) On the driving processes of the Atlantic meridional overturning circulation. Rev Geophys 45(RG2001). doi:10.1029/2004RG000166

Levitus S, Boyer TP (1994) World ocean atlas 1994. In: NOAA atlas NESDIS 4, vol 4: temperature. US Dept of Commerce, Washington DC

Levitus S, Burgett R, Boyer TP (1994) World ocean atlas 1994. In: NOAA atlas NESDIS 3, vol 3: salinity. US Dept of Commerce, Washington DC

Matsumoto K, Takanezawa T, Ooe M (2000) Ocean tide models developed by assimilating Topex/Poseidon altimeter data into hydrodynamical model: a global model and a regional model around Japan. J Oceanogr 56(5):567–581

Morozov EG (1995) Semidiurnal internal wave global field. Deep Sea Res Part I 42(1):135–148

Munk WH (1981) Internal waves and small-scale processes. In: Warren BS, Wunsch C (eds) Evolution of physical oceanography. MIT Press, Cambridge

Munk WH, Wunsch C (1998) Abyssal recipes II: energetics of tidal and wind mixing. Deep Sea Res Part I 45(12):1977–2010

Nakamura T, Isoda Y, Mitsudera H, Takagi S, Nagasawa M (2010) Breaking of unsteady lee waves generated by diurnal tides. Geophys Res Lett 37(L0462). doi:10.1029/2009GL041456

Niwa Y, Hibiya T (2004) Three-dimensional numerical simulation of M_2 internal tides in the East China Sea. J Geophys Res 109(C04027). doi:10.1029/2003JC001923

Nycander J (2005) Generation of internal waves in the deep ocean by tides. J Geophys Res 106(C10028). doi:10.1029/2004JC002487

Pacanowski RC, Philander SGH (1981) Parameterization of vertical mixing in numerical models of tropical oceans. J Phys Oceanogr 11(11):1443–1451

Schmitz WJ (1995) On the interbasin-scale thermohaline circulation. Rev Geophys 33(2):151–174

Simmons HL, Hallberg RW, Arbic BK (2004) Internal wave generation in a global baroclinic tide model. Deep Sea Res Part II 51(25–26):3043–3068

Sjöberg B, Stigebrandt A (1992) Computations of the geographical distribution of the energy flux to mixing processes via internal tides and the associated vertical circulation in the ocean. Deep Sea Res Part A 39(2A):269–291

Smith WHF, Sandwell DT (1997) Global sea floor topography from satellite altimetry and ship depth soundings. Science 277(5334): 1956–1962

St. Laurent LC, Simmons HL, Jayne SR (2002) Estimating tidally driven mixing in the deep ocean. Geophys Res Lett 29(2016). doi:10.1029/2002GL015633

Tanaka Y, Hibiya T, Niwa Y, Iwamae N (2010) Numerical study of K_1 internal tides in the Kuril Straits. J Geophys Res 115 (C09016). doi:10.1029/2009JC005903

Webb DJ, Suginohara N (2001) Vertical mixing in the ocean. Nature 409(6816):37

Zhai X, Greatbatch RJ, Eden C, Hibiya T (2009) On the loss of wind-induced near-inertial energy to turbulent mixing in the upper ocean. J Phys Oceanogr 39(11):3040–3045

Zilberman N, Becker JM, Merrifield MA, Carter GS (2009) Model estimates of M_2 internal tide generation over Mid-Atlantic Ridge topography. J Phys Oceanogr 39(10):2635–2651

Journal : Large 10872 | Dispatch : 8-7-2011 | Pages : 10
Article No. : 52 | LE | TYPESET
MS Code : JO52_1293 | CP | DISK